

A numerical study of the second-order wave excitation of ship springing by a higher-order boundary element method

Yan-Lin Shao^{1,2} and Odd M. Faltinsen²

¹*Maritime Advisory, DNV GL AS*

²*Centre for Autonomous Marine Operations and Systems (AMOS),
Department of Marine Technology, NTNU, NO-7491 Trondheim, Norway*

ABSTRACT: *This paper presents some of the efforts by the authors towards numerical prediction of springing of ships. A time-domain Higher Order Boundary Element Method (HOBEM) based on cubic shape function is first presented to solve a complete second-order problem in terms of wave steepness and ship motions in a consistent manner. In order to avoid high order derivatives on the body surfaces, e.g. m_j -terms, a new formulation of the Boundary Value Problem in a body-fixed coordinate system has been proposed instead of traditional formulation in inertial coordinate system. The local steady flow effects on the unsteady waves are taken into account. Double-body flow is used as the basis flow which is an appropriate approximation for ships with moderate forward speed. This numerical model was used to estimate the complete second order wave excitation of springing of a displacement ship at constant forward speeds.*

KEY WORDS: Springing; Weakly nonlinear; Time domain; Boundary element method.

INTRODUCTION

Springing of ships is a steady-state wave-induced global hydroelastic resonant vibration, while whipping is a transient and decaying vibration caused by impulsive loading (i.e. slamming). The linear and nonlinear springing loads on ships may strongly reduce the fatigue life of ships. Storhaug (2007) documented that the springing and whipping may contribute to approximately 50% of the accumulated fatigue damage based on full-scale measurements of a 300 m bulk carrier. Wave-induced extreme hull girder loading causes important nonlinearities in the design wave bending moment amidships. See Jensen (2000).

Linear springing of ships in regular waves occurs when the frequency of encounter matches the natural frequency of 2-node vibration. It implies that the response has the same frequency as the encounter frequency of the incident wave. Skjördal and Faltinsen (1980), Bishop et al. (1977) and Maeda (1980) developed linear springing theories. Skjördal and Faltinsen (1980) considered head sea and modified Faltinsen's (1971) short wavelength theory, which accounts for important 3D flow effects. They found the hydrodynamic forces by solving the diffraction problem and integrate the pressure over the hull surface. Bishop et al. (1977) and Maeda (1980) found these forces by formulating a reciprocity relationship and solving the radiation (forced oscillation) problem.

Nonlinear springing has also been observed in regular waves in model tests (see e.g. Storhaug, 2007; Slocum and Troesch, 1983; Miyake et al., 2008) when the encounter frequency is equal to $1/n$ of the structural natural frequencies where n is integer,

Corresponding author: Yan-Lin Shao, e-mail: shao.yanlin1981@gmail.com

This is an Open-Access article distributed under the terms of the Creative Commons Attribution Non-Commercial License (<http://creativecommons.org/licenses/by-nc/3.0>) which permits unrestricted non-commercial use, distribution, and reproduction in any medium, provided the original work is properly cited.

i.e. we can talk about second-order, third-order and so on nonlinearly excited springing. If we consider an irregular sea, second-order springing is associated with sum-frequency effects. Wu et al. (1997) has proposed a 3D nonlinear hydroelasticity theory, where the contributions of the first-order wave potentials and responses to the second-order hydrodynamic actions on a flexible body were formulated. The nonlinearities in the free-surface conditions are not considered. Tian and Wu (2006) has applied this theory to ships traveling in random waves, with a constant forward speed. Vidic-Perunovic and Jensen (2005) studied theoretically non-linear springing due to bidirectional waves. The incident waves are described consistently by second-order theory while a pragmatic second-order strip theory is used to describe the interaction with the ship. The effect of non-linear cross-coupling terms between two long-crested wave systems was added to the second-order terms from each of the two wave systems alone. This was shown to significantly influence the springing-induced response.

It is hard from a numerical point of view to go beyond second-order nonlinearly excited springing by a consistent perturbation scheme. Further, a perturbation scheme becomes increasingly tedious with increasing order of nonlinearly excited springing. If the body surface at rest is not vertical at the free surface, difficulties with flow singularities at the intersections between the mean free surface and body occur. The latter fact limits the possibilities in analyzing higher order than second-order problems for ships with bow flare. When a tank has non-vertical surface in the free-surface zone, Faltinsen and Timokha (2014) demonstrated for the linear eigenvalue problem that singular solutions had to be added at the intersections between the mean free surface and the tank surface to obtain high accuracy in predicting natural sloshing frequencies.

It is now commonly accepted that springing can be excited not only by the linear wave loads but also nonlinear wave loads. Miyake et al. (2008) found experimentally for a modified Wigley model that the springing of super harmonic (n-th) resonance due to the higher-order nonlinear hydrodynamic forces occurred, although the model is a simple mathematical hull form without bulbous bow. The similar phenomenon has been reported by Storhaug (2007) in his model tests of a bulk carrier with different bow shapes.

The wave-induced sectional loads on ships are often analyzed by a blended method, which is based on the linear solution with nonlinear corrections for the Froude-Krylov and the restoring forces. von Graefe et al. (2014) considered the weak nonlinearity of the sectional loads in waves (e.g., hogging-sagging asymmetry) by pressure extrapolation and integration up to the estimated actual water line. Slamming-type of loads may also be added by, for instance, the 2D and 3D generalized Wagner approaches. See Zhao et al. (1996) and Faltinsen and Chezhian (2005). In the generalized Wagner models, the free-surface conditions are the same as in Wagner's outer flow domain, i.e. the dynamic condition is zero velocity potential and the kinematic condition is fully nonlinear. The body-boundary condition is satisfied on the exact body boundary. It is required in the generalized Wagner method that the lateral coordinates of the intersection between body surface and free surface must not decay with time. Therefore, it is not consistent to use the Generalized Wagner approaches in the water exit. Highly accurate and efficient numerical methods to solve the 2D generalized Wagner problem have been developed by, for instance, Helmers and Skeie (2013), Khabakhpasheva et al. (2014) and Korobkin (2011). The coupled seakeeping and 2D generalized Wagner model has been studied by Tuitman and Malenica (2009) and it was shown to be a useful approach from engineering point of view. Further improvements in such coupled model are needed to, for instance, properly take into account the forward speed effects and avoid double counting of the wave forces from wave radiation. In the blended methods, the nonlinearities in the wave radiation and diffraction are only partly considered. How important the neglected nonlinear wave radiation/diffraction is as the excitation of nonlinear ship springing still remains as a mystery. In order to answer this question, it is necessary to solve a complete higher-order problem (e.g. second-order problem) with the presence of forward speed.

The Boundary Value Problems (BVPs) for the linear and higher-order potential-flow solutions for external flows are traditionally formulated in an inertial coordinate system. The body-boundary and free-surface conditions are by Taylor expansions formulated on the mean body and free-surface positions. Because the steady flow does not satisfy the body-boundary condition on the instantaneous body surface, the important m_j -terms occur in the linear body-boundary conditions for ship motions at forward speed. The second-order solution involves second-order derivatives of the first-order unsteady velocity potential and second-order and third-order derivatives of the steady velocity potential on the mean body surface. If the body has sharp corners with interior angles less than 180° , the procedure fails at the sharp corners and flow singularities occur. Use of a body-fixed coordinate system in solving higher-order potential-flow problems does not include any derivatives of the velocity potential on the right-hand side of the body-boundary conditions. Shao and Faltinsen (2010; 2012a; 2012b; 2013; 2014) formulated the boundary value problem in the body-fixed coordinate system in the analysis of the weakly nonlinear wave-

body interaction problems without and with forward speed/current velocity. Shao and Faltinsen (2012a) found for a Wigley hull that the second-order velocity potential gives dominant contribution to the second-order wave excitation of ship springing in the wave frequency region where sum-frequency springing occurs. A two-node vertical structural mode was considered. The blended methods for nonlinear wave-induced loads on ships at forward speed represent state-of-the-art engineering tools and give wrong results because nonlinearities in the wave radiation and diffraction are not considered. The double-body flow is used as the basis flow. Both monochromatic and bichromatic head-sea waves are considered with different Froude numbers. A time-domain higher-order BEM (HOBEM) based on cubic shape functions is used and a forward difference scheme is applied in the free-surface conditions in order to better numerically stabilize the solution. A modified 4th order Runge Kutta method, which takes care of the convective terms in the free surface conditions was recently proposed by Shao and Helmers (2014) in the time integration of the free surface conditions to further stabilize the time domain solutions. Generalization to semi-displacement vessels implies that flow separation from the transom stern with a hollow in the water behind must be incorporated. In this article, the time-domain HOBEM with a formulation of BVP in body-fixed coordinate system will be presented, followed by numerical studies of second-order wave excitation of springing of modified Wigley hulls in both monochromatic and bichromatic waves.

SECOND-ORDER WEAKLY NONLINEAR BVP IN BODY-FIXED COORDINATE SYSTEM

Definition

As shown in Fig. 1, we define four right-handed Cartesian coordinate systems, i.e. $O_e X_e Y_e Z_e$, $OXYZ$, $oxyz$ and $o_g x_g y_g z_g$. $O_e X_e Y_e Z_e$ is Earth-fixed with $X_e Y_e$ -plane on the calm water surface and the Z_e -axis positive upwards. $OXYZ$ is an inertial coordinate system moving with the steady forward speed of the body. The XY -plane coincides with the $X_e Y_e$ -plane and the Z -axis parallel to the Z_e -axis. $oxyz$ is a body-fixed coordinate system which moves with not only the steady forward speed but also the unsteady rigid-body motions of the body. The z -axis goes through the center of gravity (COG). When the body is without unsteady motions, $oxyz$ coincides with $OXYZ$ with the origin on the mean free surface. The $o_g x_g y_g z_g$ is an inertial coordinate system with origin located on the COG, with its axis parallel to that of $OXYZ$. The body is normally assumed to have the oxz -plane as a plane of symmetry.

Let us define the translatory motion vector of the origin of $oxyz$ relative to the origin of $OXYZ$, i.e. \overline{Oo} , be $\vec{\xi} = (\xi_1, \xi_2, \xi_3)$ so that ξ_1 is the surge, ξ_2 is the sway and ξ_3 is the heave. In addition, we define the Euler angles α_4 , α_5 and α_6 about the X -, Y - and Z -axis respectively so that α_4 is the roll, α_5 is the pitch and α_6 is the yaw.

When the water is assumed incompressible and inviscid, and the flow is irrotational, the water motion can be described by a scalar ϕ which is defined as the velocity potential. ϕ satisfies the Laplace equation

$$\nabla^2 \phi = 0 \text{ in the water domain.} \tag{1}$$

The water has infinite horizontal extent and depth. The amplitudes of the incident waves and the oscillatory body motions relative to the characteristic body dimensions are assumed asymptotically small in the incident wave slope.

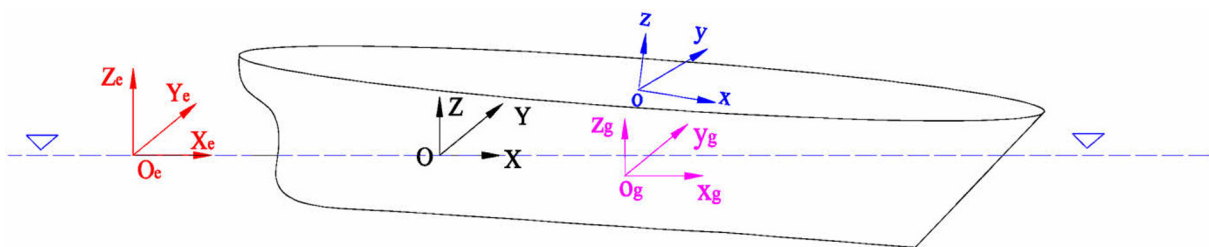


Fig. 1 Definition of different coordinate systems.

Formulation of boundary value problem (BVP) in the body-fixed coordinate system

This section briefly shows the first order and second order free-surface and body-boundary conditions in the body-fixed coordinate system. The following notation will be used through this section: A vector with a prime is described in the body-fixed coordinate system. Otherwise, the vector is a description in the inertial reference frame.

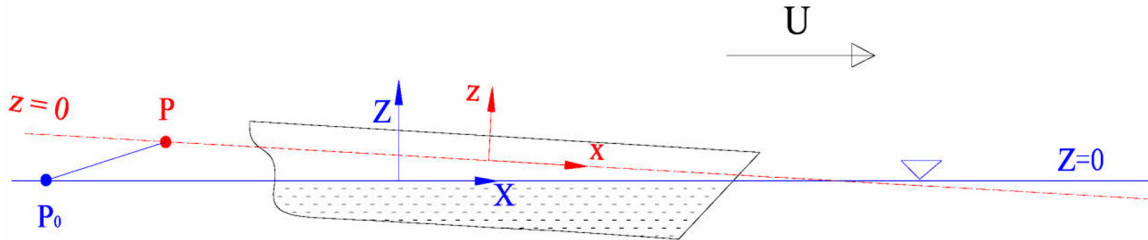


Fig. 2 The relationship between the calm-water surface and the xy-plane.

The fully-nonlinear formulation of the free-surface conditions in a non-inertial coordinate system can be found in, for instance Faltinsen and Timokha (2009), as

$$\eta_t = \phi_z - \phi_x \eta_x - \phi_y \eta_y - (\bar{U}' + \dot{\xi}' + \bar{\omega}' \times \bar{r}') \cdot (-\eta_x, -\eta_y, 1) \quad \text{on } z = \eta(x, y, t), \tag{2}$$

$$\phi_t = -\frac{1}{2} \nabla \phi \cdot \nabla \phi + (\bar{U}' + \dot{\xi}' + \bar{\omega}' \times \bar{r}') \cdot \nabla \phi - U_g \quad \text{on } z = \eta(x, y, t). \tag{3}$$

Here the subscripts $x, y, z,$ and t indicates partial differentiation. $\bar{r}' = (x, y, \eta)$ is the position vector of a point on the free surface. $\dot{\xi}'$ and $\bar{\omega}'$ are translatory and rotary body motions, respectively. All the vectors are described in the body-fixed coordinate system, i.e. $oxyz$ in Figs. 1 and 2. The gradients are taken with respect to x, y and $z,$ i.e. $\nabla = \bar{i} \frac{\partial}{\partial x} + \bar{j} \frac{\partial}{\partial y} + \bar{k} \frac{\partial}{\partial z}.$ U_g is the gravity potential. For a point $\bar{r}' = (x, y, \eta)$ on the free surface, U_g can be expressed as

$$U_g = -\bar{g} \cdot [\bar{\xi} + \mathbf{R}_{b \rightarrow i} \bar{r}'] \tag{4}$$

where $\bar{g} = -g\bar{K}.$ $\bar{\xi} = \xi_1 \bar{I} + \xi_2 \bar{J} + \xi_3 \bar{K}$ is the translatory motion vector of the origin of $oxyz$ relative to $OXYZ$ system. \bar{I}, \bar{J} and \bar{K} are unit vectors along $X-, Y-$ and $Z-$ axis, respectively. The transformation matrix $\mathbf{R}_{b \rightarrow i}$ that transforms the representation of a vector in the body-fixed $oxyz$ system to its representation in the inertial $OXYZ$ system is defined in Appendix A. 'b' and 'i' in the subscript means body-fixed frame and inertial coordinate system, respectively.

The free-surface conditions (2) and (3) are then approximated by introducing Stokes expansion and Taylor expanding of the free-surface conditions about the oxy -plane. One should note that the oxy -plane is not necessarily the same as the calm water surface, i.e. the OXY -plane in Figs. 1 and 2. The oxy -plane coincides with the calm water surface when the body is at rest, and translates and rotates with the body. As shown in Fig. 2, a point P_0 initially on the calm water surface will move to point P due to unsteady rigid-body motions. Since the computational domain will be truncated at a finite distance from the body in the following time-domain HOBEM analysis, the displacement of a point fixed on the oxy -plane (e.g. $|P_0P|$ in Fig. 2) will always be small compared with the dimensions of the ship, which is a necessary in the Stokes expansion and Taylor expansion.

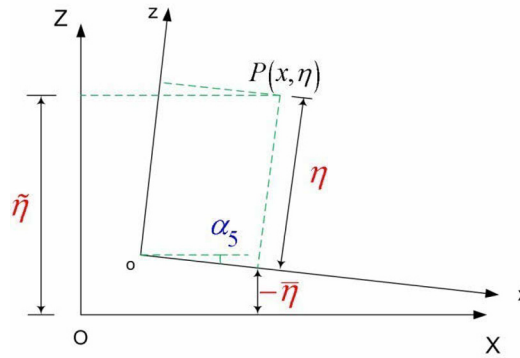


Fig. 3 Definition of the wave elevations observed in the body-fixed coordinate system oxyz and the inertial coordinate system OXYZ.

The free-surface elevation observed in the body-fixed coordinate system has two contributions. The first part is due to the rigid-body motions. It can be understood as follows. When the water is calm, i.e. no incoming or scattered waves, the calm water surface has a relative motion observed in the body-fixed reference frame due to the unsteady body motions. The other contribution is associated with the wave motion with the mentioned rigid-body motion effect excluded. Fig. 3 shows a two-dimensional sketch of the definition of the wave elevation $\tilde{\eta}$ observed in the inertial coordinate system OXYZ and the wave elevation η observed in the body-fixed coordinate system oxyz. $P(x, \eta)$ is a point on the instantaneous free surface. $(-\bar{\eta})$ is the displacement of a point $(x, y, 0)$ on the oxy-plane due to the rigid-body motions. α_5 is the pitch angle of the body. Keeping in mind that the rigid-body motions and the wave elevation are small, we can approximate the relationship between η and $\tilde{\eta}$ as

$$\eta = \bar{\eta} + \tilde{\eta} + O(\varepsilon^3). \tag{5}$$

From a numerical point of view, it was found advantageous to use the decomposition in Eq. (5) and to operate with $\tilde{\eta}$ instead of η in the free-surface conditions.

By introducing the Stokes expansion of the velocity potential ϕ , wave elevation η , translational body motion $\vec{\xi}$ and rotational body motion $\vec{\alpha}$, Taylor expansion of the free-surface conditions about the oxy-plane of the body-fixed coordinate system, and collecting consistent terms at different orders, we can get the following free-surface conditions

$$\tilde{\eta}_t^{(m)} = \phi_z^{(m)} + f_1^{(m)} \quad \text{on } z=0, \tag{6}$$

$$\phi_1^{(m)} = -g\tilde{\eta}^{(m)} + f_2^{(m)} \quad \text{on } z=0, \tag{7}$$

with the forcing terms $f_1^{(m)}, f_2^{(m)}$ ($m=1, 2$) defined in the Appendix B.

The double-body flow is used as the basis flow, which has a different interpretation but the same solution as that in an inertial coordinate system. See Shao and Faltinsen (2012b) and Shao (2010) for details.

The body-boundary condition in the body-fixed coordinate system is

$$\phi_n^{(m)} = b^{(m)}, \quad m=1, 2, \quad \text{on SB.} \tag{8}$$

SB is the body surface at the instantaneous position of the body. Only the mean wetted part of the body surface is used in the formulation. The effect of small variation of the wetted body surface due to the wave elevation and rigid body motion will be handled by the Taylor expansion about the oxy-plane of the body-fixed coordinate system. This is valid as long as the body motion and wave elevation are small relative to the body’s cross-dimensional lengths.

The forcing term $b^{(m)}$ ($m=1, 2$) is defined as

$$b^{(1)} = \vec{n}' \cdot \left(\vec{\xi}'^{(1)} + \vec{\omega}'^{(1)} \times \vec{r}' + \vec{U}'^{(1)} \right), \quad (9)$$

$$b^{(2)} = \vec{n}' \cdot \left(\vec{\xi}'^{(2)} + \vec{\omega}'^{(2)} \times \vec{r}' + \vec{U}'^{(2)} \right), \quad (10)$$

where $\vec{\xi}'^{(i)}$ and $\vec{\omega}'^{(i)}$ ($i=1, 2$) are the translatory and angular velocity vectors of the body expressed in the body-fixed coordinate system. $\vec{U}'^{(k)}$ ($k=1, 2$) is k -th order component of the steady forward speed vector in the body-fixed coordinate system defined in Eq. (B.7). \vec{n}' is the normal vector on the body surface. $\vec{r}' = (x, y, z)$ is the position vector of a point on the body surface.

The body-boundary condition is formulated on the instantaneous position of the body surface. The latter fact avoids introduction of e.g. the mj-terms. In the analysis presented in this paper, we will focus on wave excitation for springing of ships in either regular waves or bichromatic waves where the frequencies of the wave components are close. The wavelength ranges that cause first-order, second-order and higher-order resonant springing are different. Taking a 300 meters ship length travelling in headsea with forward speed 10 *m/s* as an example and assuming the highest natural period as 2 *sec.*, one can estimate that the resonant linear, sum-frequency and triple-frequency resonant springing are caused by waves with wavelengths 0.12 *L*, 0.29 *L* and 0.51 *L* respectively. Here *L* is the ship length. The waves with 0.29 *L* as the wavelength will not excite the resonant springing of the ship when only linear wave loads are considered. That means that when considering second-order springing, we do not have to consider the effect of first-order springing in the formulation of the boundary value problem. Even though the rigid-body motions will typically be small in the wavelength range of second-order excited springing, we will include this effect to illustrate the use of body-fixed coordinate system. The velocity potential ϕ in this section is the absolute velocity potential, which is different from the relative velocity potential.

TIME-DOMAIN HIGHER ORDER BOUNDARY ELEMENT METHOD (HOBEM)

A time-domain HOBEM based on cubic shape functions is used to solve the Boundary Integral Equation (BIE), which is the consequence of using Green's 3rd identity in the computational fluid domain. The Rankine source (or simple $1/r$ with r as the distance between source and field point) is chosen as the Green function. Dipoles and sources (or sinks) with unknown strengths are distributed on the free surface and the body surface, respectively. The computational domain is truncated at a certain distance away from the ship and a damping zone is applied at the outer layer of the free surface, so that most of the energy of the scattered waves is damped out when they travel through the damping zone.

An explicit 4th-order Runge-Kutta (RK4) method is applied in the time integration of the free-surface conditions. At each time step, the velocity potential is known on the free surface while the normal velocity is given by the body-boundary conditions. Consequently, the HOBEM solver provides normal velocity and velocity potential on the free surface and body surface, respectively.

In the time-domain simulation of the free-surface waves, two sorts of instabilities are seen when time-integrating the free-surface conditions. The first instability leads to continuously increasing wave amplitudes destroying the solution. The other one leads to stable saw-tooth behavior of small wave lengths. In Shao and Faltinsen (2012a; 2012b), the first instability is avoided by choosing a proper combination of the time-marching scheme and the Finite Difference (FD) schemes for the spatial derivatives.

In order to find a scheme with larger stability region, the Fourier-von Neumann stability analysis for different FD schemes combined with the time-marching schemes has been applied by Shao and Faltinsen (2012a; 2012b). The non-dimensional linearized free-surface conditions without steady velocity potential and the body motion effects are considered in the stability analysis as a first approximation. Other matters, e.g. the aspect ratio of elements and the presence of steady velocity potential, which are not considered in the stability analysis, will also influence the stability. Based on the stability analysis, it was then

decided to use 3-point upwind FD scheme for the longitudinal derivative terms in the free-surface conditions. The other derivatives are still based on cubic shape functions. Recently, Shao and Helmers (2014) proposed an improved Runge-Kutta 4th scheme for the time integration of free surface conditions by treating the convective terms in the free surfaces in an implicit way. This improved scheme was shown to be more stable than the previously used 4th order explicit Runge-Kutta scheme.

In order to suppress the stable saw-tooth behavior, a low-pass filter is implemented and applied on the collocation points at the waterline and on points adjacent to these. In this study, a three-point low-pass filter is adopted

$$\bar{w}_j = cw_{j-1} + (1-2c)w_j + cw_{j+1}. \quad (11)$$

Here j is a local numbering of the collocation points in the longitudinal or transverse direction. c is the strength of the filter. w_j and \bar{w}_j are either the velocity potential or the wave elevation before and after smoothing. This low-pass filter was applied by Büchmann (2000) successfully in the second-order wave diffraction with a weak current based on linear BEM, and later by Shao (2010) in second-order radiation/diffraction with small forward speeds based on time-domain HOBEM.

Taking the Fourier transformation of the filter in Eq. (11) enables us to study the damping effects of the low-pass filter for different wave lengths. The results for $c=0.04, 0.08$ and 0.12 are presented in Fig. 4. For example, the low-pass filters with $c=0.04, 0.08$ and 0.12 damp the amplitude of the linear wave with wave length $20\Delta x$ by 0.392%, 0.783% and 1.175%, respectively. Δx is the element size of a uniform grid. Correspondingly, they reduce the amplitude of the short wave (with wave length $2\Delta x$) by 16%, 32% and 48%, respectively.

In this article, the low-pass filter is applied to the first and second order wave elevations with filter strength $c=C1\approx 0.0-0.04$ and the spatial derivatives of the first order quantities in the second-order forcing terms (i.e. Eq. (B.3) and Eq. (B.4)) with filter strength $c=C2\approx 0.04-0.12$. The low-pass filter is applied at each time step in order to suppress the possible growth and propagation of the numerical short waves.

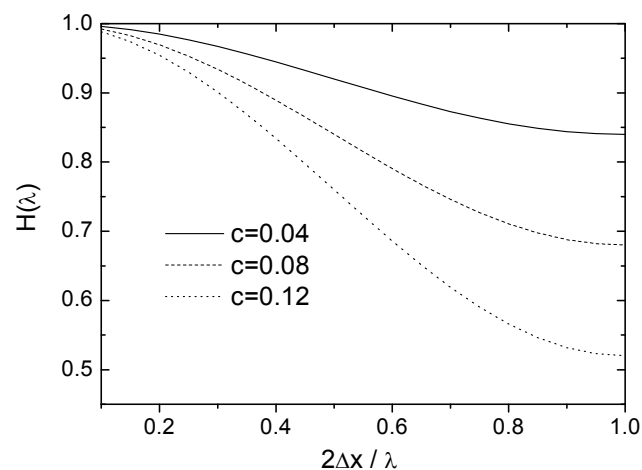


Fig. 4 Low-pass filters in Eq. (11) for spatial smoothing.

SECOND-ORDER WAVE EXCITATION OF SPRINGING OF A MODIFIED WIGLEY HULL

Second-order wave excitation of springing of ships in monochromatic waves and bichromatic waves are studied. Modified Wigley hull in head-sea waves is considered. The modified Wigley hull is a simple mathematical ship form without bulbous bow. However, it has been reported by Miyake et al. (2008) that nonlinear springing occurred on this ship form.

The hull is mathematically described as

$$\zeta_2 = (1-\zeta_3)^2 (1-\zeta_1)^2 (1+0.2\zeta_1^2) + \zeta_3 (1-\zeta_3^8)(1-\zeta_1^2)^4, \quad -1 \leq \zeta_1 \leq 1, -1 \leq \zeta_3 \leq 0, \quad (12)$$

with

$$\{x, y, z\} = \{0.5\zeta_1 L, 0.5\zeta_2 B, \zeta_3 D\} \quad (13)$$

An example of the meshes on half of the free surface and wetted mean ship hull is shown in Figs. 5(a) and (b), respectively. In order to use the upwind schemes for the spatial derivatives, we have adopted rectangular mesh resolution on the free surface. The meshes are finer near the waterline and gradually become coarse away from the ship.

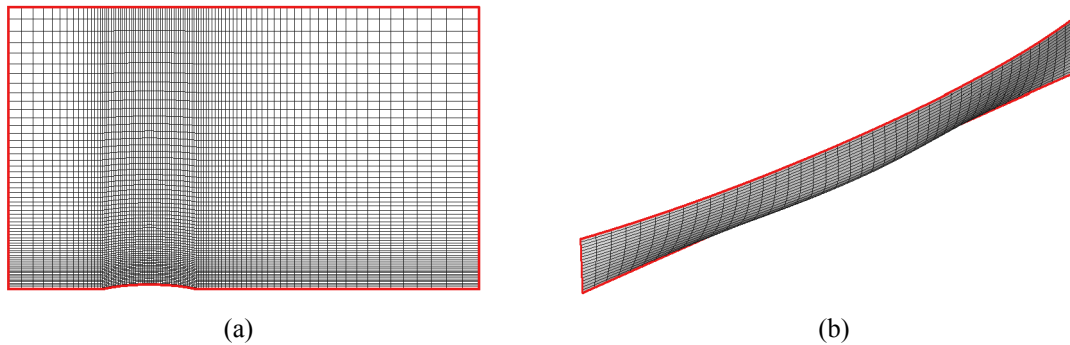


Fig. 5 Meshes on the free surface and the wetted mean ship surface. Due to symmetric properties, only half of the free surface and ship surface are discretized. (a) Meshes on the half of the free surface. (b) Meshes on half of the Wigley hull.

For given ship length (L), Froude number (Fr), wave heading and structural natural frequencies (ω_n), one can estimate the corresponding wave length when the second-order ship springing occurs. Considering a 300 m ship whose lowest structural natural period is typically around 2 sec., travelling in head-sea waves with $Fr < 0.3$, we found that the second-order ship springing only occurs in the relatively short wave region, e.g. $\lambda/L \leq 0.3$. λ is the linear incident wave length.

As a starting point, we have studied the second-order wave diffraction of the modified Wigley hull traveling in the regular head-sea waves with $0.25 \leq \lambda/L \leq 0.5$. This enables us to identify the relative importance of the quadratic effects of the linear solution and the second-order velocity potential, as the sources of the excitation of nonlinear ship springing. One should note that, springing is a resonant phenomenon, in which the damping sources can be as equally important as the excitation. The discussion on different sources of damping effects can be found in Söding (2009). However, the wave excitation is the only focus of this study.

The generalized second-order vertical excitation force of the 2-node mode in the vertical plane is investigated, which is defined as

$$F_7^{(2)} = \iint_{SB} P^{(2)}(x, y, z) n_3^{(0)}(x, y, z) \psi(x) ds \quad (14)$$

Here $n_3^{(0)}$ is the z -component of the normal vector of the ship hull. Because the modified Wigley ship studied in this article has vertical surface at the mean waterline, a waterline integral has been neglected in Eq. (14). $\psi(x)$ is the normalized 2-node dry structural mode in the vertical plane, defined as

$$\psi(x) = \frac{2}{\sqrt{L[\cosh(aL) - \cos(aL)]}} \left[\cos(ax) \sinh\left(\frac{aL}{2}\right) - \cosh(ax) \sin\left(\frac{aL}{2}\right) \right] \quad (15)$$

where L is ship length. a is the lowest root of

$$\tan\left(\frac{aL}{2}\right) = -\tanh\left(\frac{aL}{2}\right), \quad a > 0. \tag{16}$$

The mode $\psi(x)$ in Eq. (15) was normalized to satisfy

$$\int_L \psi(x) \cdot \psi(x) dx = 1. \tag{17}$$

As the first example, the modified Wigley ship defined in Eqs. (12)-(13) is scaled to full scale with ship length, beam and draft as $L=300\text{ m}$, $B=30\text{ m}$ and $D=18.75\text{ m}$ respectively. Presented in Fig. 6 are the results for $Fr=0.18, 0.20$, and 0.22 . $F_{7,a}^{(2)}$ is the amplitude of the total generalized second-order excitation of the 2-node mode in the vertical plane. $F_{7,p2}^{(2)}$ and $F_{7,q}^{(2)}$ are the contributions from the second-order velocity potential and the quadratic velocity terms in the Bernoulli's equation, respectively. It is immediately apparent that the second-order velocity potential gives dominant contributions relative to the quadratic velocity terms. This is somewhat similar to what we have learnt in the analysis of second-order wave diffraction on a fixed hemisphere. For a submerged hemisphere restrained in waves, Kim (1988) demonstrated that the contribution of second-order velocity potential dominates over the quadratic velocity term in the Bernoulli's equation in the short wave region, and that it may not be conservative to simply neglect the second-order velocity potential effects in the nonlinear wave diffraction forces analysis. Since only regular waves with infinite water depth are studied in this case, the second order incident wave potential is zero thus has no contribution to the excitation of ship springing. Furthermore, the comparison of the results for different Froude numbers ($Fr=0.18, 0.20, 0.22$) also suggests that the second-order excitation has a strong dependence on the Froude number for small wave lengths.

Actually, a ship with $L=300\text{ m}$, $B=30\text{ m}$ and $D=18.75\text{ m}$ represents an unusual ship. Therefore, two other ships with different beam and draft are also studied, both of which are scaled from the modified Wigley ship defined in Eqs. (12)-(13). The first ship has $L=300\text{ m}$, $B=48\text{ m}$ and $D=18.75\text{ m}$ and the other one is with $L=300\text{ m}$, $B=48\text{ m}$ and $D=11\text{ m}$. The selection of the ship size is based on a bulk carrier studied by Storhaug (2007). The deep and shallow drafts represent cargo and ballast conditions, respectively. $Fr=0.18$ is considered. The results for second-order excitation of springing are shown in Fig. 7. Comparing

Figs. 1 and 7, we see that the blunt ship suffers higher second-order springing excitation relative to the slender ship. This may be explained by the fact that blunt ship generates stronger scattered wave, which in return interacts with the incident wave and itself to give second-order effects. The comparison also indicates higher second-order excitation for ship in ballast load condition than full load condition, in which case it is easier for the ship bottom to feel the incident wave and cause disturbance. Furthermore, the relative contribution of the quadratic velocity term in Bernoulli's equation has increased in ballast condition. However, in the studied wave length region, its contribution is still smaller than that of the second-order velocity potential.

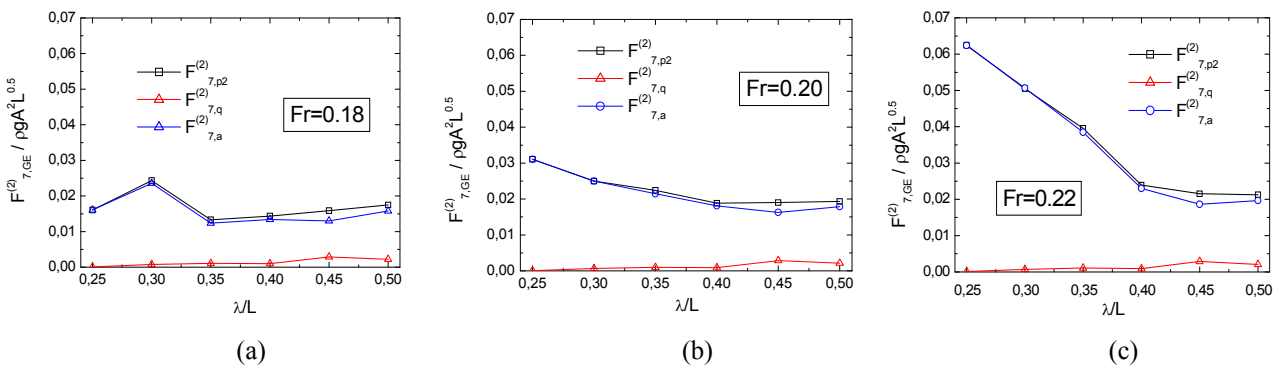


Fig. 6 The second-order generalized excitation of the 2-node vertical mode for a modified Wigley hull ($L=300\text{ m}$, $B=30\text{ m}$, $D=18.75\text{ m}$) in regular head-sea waves. The ship is restrained from unsteady motions. (a) $Fr=0.18$. (b) $Fr=0.20$. (c) $Fr=0.22$.

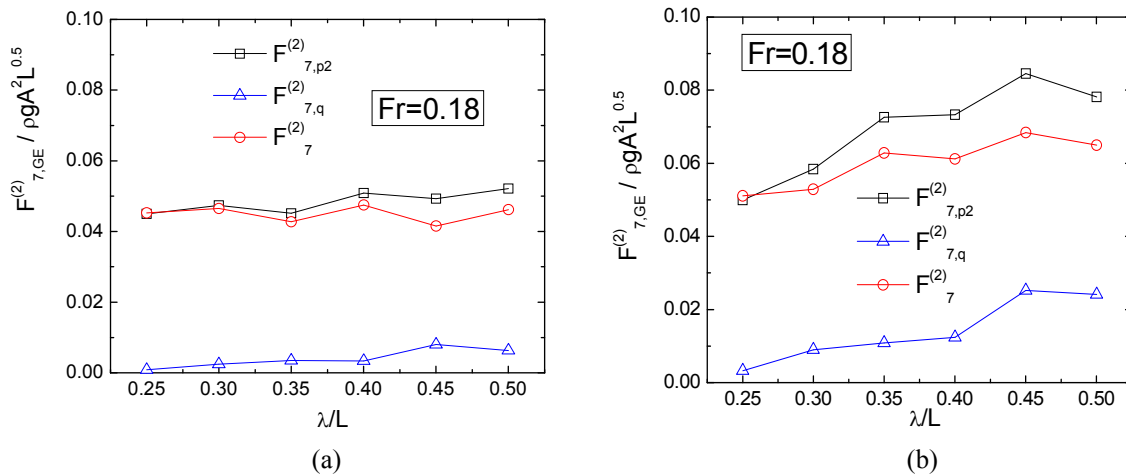


Fig. 7 The second-order generalized excitation of the 2-node vertical mode for a modified Wigley hull in regular head-sea waves. The ship is restrained from unsteady motions. $Fr=0.18$. (a) $L=300\text{ m}$, $B=48\text{ m}$, $D=18.75\text{ m}$; (b) $L=300\text{ m}$, $B=48\text{ m}$, $D=11\text{ m}$.

When a ship travels in the seaway, the incident waves are irregular containing infinite number of wave components. Evaluation of second-order sum-frequency wave excitation of ship springing in irregular waves is relevant to the fatigue analysis of the ships.

We consider head sea and assume long-crested waves with a wave energy spectrum $S_e(\omega_e)$ with respect to the encounter frequency ω_e . In general, the total sum-frequency generalized excitation of springing can be written as

$$F_7^{(2)} = \sum_{i=1}^N \sum_{j=1}^N A_i A_j T^+ (\omega_{e,i}, \omega_{e,j}) \cos [(\omega_{e,i} + \omega_{e,j})t + (\beta_i + \beta_j) + \varepsilon^+ (\omega_{e,i}, \omega_{e,j})] \tag{18}$$

Here A_i and A_j are incident wave amplitudes of frequency components no. i and j , respectively. $\omega_{e,i}$ and $\omega_{e,j}$ are wave frequencies of encounter. β_i and β_j are the random phase angles of incident waves. $\varepsilon^+ (\omega_{e,i}, \omega_{e,j})$ is the phase angle of the generalized excitation due to nonlinear interactions between the i -th wave component, the j -th wave component and the diffracted and radiated waves by the ship. T^+ is the Quadratic Transfer Functions (QTFs) with the wave elevations as input and the generalized excitation force as output. The following symmetry conditions are assumed:

$$T^+ (\omega_{e,i}, \omega_{e,j}) = T^+ (\omega_{e,j}, \omega_{e,i}) \tag{19}$$

$$\varepsilon^+ (\omega_{e,i}, \omega_{e,j}) = \varepsilon^+ (\omega_{e,j}, \omega_{e,i}) \tag{20}$$

A sum-frequency spectral density for the second-order sum-frequency excitation of springing is defined as

$$S^+ (\Omega) = 8 \int_0^{0.5\Omega} S_e (0.5\Omega - \Lambda) S_e (0.5\Omega + \Lambda) |T^+ (0.5\Omega - \Lambda, 0.5\Omega + \Lambda)|^2 d\Lambda . \tag{21}$$

Here $\Omega \geq 0$ and $2\Lambda \geq 0$ are the sum frequency and difference frequency of two wave components from the wave spectrum $S_e(\omega_e)$, respectively. Therefore, $0.5\Omega - \Lambda$ and $0.5\Omega + \Lambda$ are the encounter frequencies of the two waves. Winterstein et al. (1994) have given a similar definition for zero forward speed.

In order to get the QTFs, i.e. $T^+ (0.5\Omega - \Lambda, 0.5\Omega + \Lambda)$, we have studied the second-order sum-frequency wave excitation of ship springing in bichromatic waves. The linear wave amplitudes of the two wave components are assumed to be same in all the

analysis. This does not matter since the QTFs are independent of the incident wave amplitudes. In the simulations, we have set the random phase angles β_i and β_j in Eq. (18) equal to zero. What we obtain from this type of time-domain analysis is a time history containing several different frequencies. Specifically, the second-order components may oscillate with circular frequencies $2(0.5\Omega - \Lambda)$, $2(0.5\Omega + \Lambda)$, Ω and 2Λ respectively, together with a mean component which does not vary with time. Fourier analysis gives the amplitudes of the sum-frequency excitation with different oscillating frequencies. When the two waves are identical, we have to divide this amplitude by 4 in order to get the correct sum-frequency QTFs for ship springing defined in Eq. (18). In case the two wave components are different, this amplitude should be divided by 2.

We consider the ship with $L=300\text{ m}$, $B=30\text{ m}$ and $D=18.75\text{ m}$. The lowest structural natural period of a real ship with $\sim 300\text{ m}$ ship length is around 2 sec . Therefore, from the wave excitation point of view, it is of interest to consider pairs of waves when the sum of encounter frequencies is close to $2\pi/2 \approx 3.14\text{ rad/s}$, i.e. $\Omega\sqrt{L/g} \approx 17.4$.

Depicted in Fig. 8(a) are the amplitudes of the second-order sum-frequency transfer function for generalized excitation of 2-node mode in vertical plane. Corresponding phase angles are shown in Fig. 8(b). Head-sea waves are considered with Froude number $Fr=0.178$. The ship is free to respond in heave and pitch. The results are presented as a function of $\Omega\sqrt{L/g}$ for various non-dimensional difference frequencies $2\Lambda\sqrt{L/g} \approx 0, 1.11$ and 1.16 , corresponding to $2\Lambda=0, 0.2\text{ rad/s}$ and 0.3 rad/s , respectively. The numerical results showed that, in the considered frequency range, T^+ is in general larger for a high sum frequency than that for a low sum frequency. On the other hand, for a fixed sum-frequency, neither T^+ nor ϵ^+ show strong variation with the considered various difference frequencies. This was not the case for the TLP in the following study. Based on calculations by Molin and Chen (1990), Winterstein et al. (1994) presented numerical results of the amplitude of the second-order transfer function for the pitch moment on the Snorre TLP, showing relatively large difference for various difference frequencies.

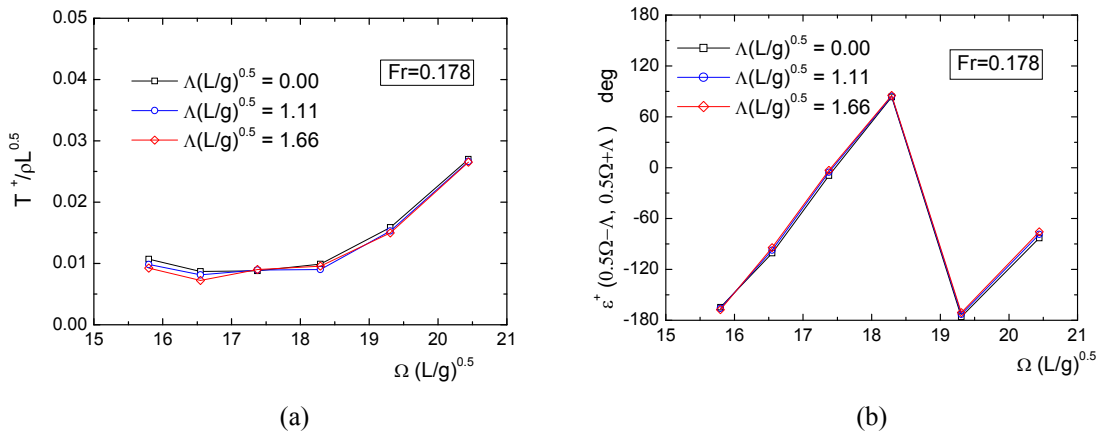


Fig. 8 Amplitudes and the phase angles of the second-order sum-frequency transfer function for generalized excitation of ship springing for a modified Wigley ship. The ship is similar to that defined in Eqs. (12)-(13), but scaled to full scale with ship length L .

SUMMARY

A time-domain Higher Order Boundary Element Method (HOBEM) based on cubic shape function has been developed to solve a complete second-order problem in terms of wave steepness and ship motions in a consistent manner. The first- and second-order boundary value problems are formulated in a body-fixed coordinate system to avoid numerical difficulties associated with higher order derivatives on body surfaces. Second-order wave excitation of springing of modified Wigley hull in both monochromatic and bichromatic waves is examined. In regular waves, different forward speed, draft and beam are studied. The second-order springing wave excitation is higher for the blunt ship than the slender one. It is also higher when the ship is in ballast loading condition than that in cargo condition. The numerical analysis also indicate that the second-order velocity potential gives dominant contribution to the second-order wave excitation of ship springing in the wave frequency region where sum-frequency springing occurs.

REFERENCES

- Bishop, R.E.D., Price, W.G. and Tam, P.K.Y., 1977. A unified dynamic analysis of ship response to waves. *Royal Institution of Naval Architects Spring Meeting*, pp.363-390.
- Büchmann, B., 2000. *Time-domain modeling of run-up on offshore structures in waves and currents*. Ph.D. thesis. Department of Hydrodynamics and Water Resources, Technical University of Denmark.
- Faltinsen, O. and Chezhian M., 2005. A generalized wagner method for three-dimensional slamming. *Journal of Ship Research*, 591(4), pp.279-287.
- Faltinsen, O.M., 1971. *Wave forces on a restrained ship in head sea waves*. Ph.D thesis. The University of Michigan.
- Faltinsen, O.M. and Timokha, A.N., 2009. *Sloshing*. Cambridge: Cambridge University Press.
- Faltinsen, O.M. and Timokha, A.N., 2014. Analytically approximate natural sloshing modes and frequencies in two-dimensional tank. *European Journal of Mechanics, B/Fluids*, 47, pp.176-187.
- Helmers, J.B. and Skeie, G., 2013. A meshless boundary element method for simulating slamming in context of generalized wagner. Odd M. Faltinsen Honoring Symposium on Marine Hydrodynamics, Nantes, France, 9-14 June 2013, pp.V009T12A046.
- Jensen, J.J., 2000. *Extreme hull girder loading, Report of ISSC committee VI.1*. Amsterdam: Elsevier.
- Khabakhpasheva, T.I., Kim, Y.H. and Korobkin, A.A., 2014. Generalised Wagner model of water impact by numerical conformal mapping. *Applied Ocean Research*, 44, pp.29-38.
- Kim, M.H., 1988. *The complete second-order diffraction and radiation solution for an axisymmetric body*. PhD Thesis. MIT.
- Korobkin, A.A., 2011. Semi-analytical approach in generalized wagner model. *26th International Workshop on Water Waves and Floating Bodies*, Greece, 17-20 April 2011.
- Maeda, H., 1980. *On the theory of coupled ship motions and vibrations, Report No.232*. Ann Arbor: The University of Michigan, Department of Naval Architecture and Marine Engineering.
- Miyake, R., Matsumoto, T., Zhu, T. and Abe, N., 2008. Experimental studies on the hydroelastic response due to springing using a flexible mega-container ship model. *8th International Conference on Hydrodynamics*, Nantes, 1-3 October 2008.
- Molin B. and Chen X. B., 1990. *Calculation of second-order sum-frequency loads on TLP hulls*. Rueil-Malmaison, France: Institute Français du Pétrole.
- Shao, Y.L., 2010. *Numerical potential-flow studies on weakly-nonlinear wave-body interactions with/without small forward speeds*. PhD thesis. Dept of Marine Technology, NTNU.
- Shao, Y.L. and Faltinsen O.M., 2010. Use of body-fixed coordinate system in analysis of weakly-nonlinear wave-body problems. *Applied Ocean Research*, 32(1), pp.20-33.
- Shao, Y.L. and Faltinsen, O.M., 2012a. A numerical study of the second-order wave excitation of ship springing with infinite water depth. *Journal of Engineering for the Maritime Environment*, 226(2), pp.103-119.
- Shao, Y.L. and Faltinsen, O.M., 2012b. Linear seakeeping and added resistance analysis by means of body-fixed coordinate system. *Journal of Marine Science and Technology*, 17, pp.493-510.
- Shao, Y.L. and Faltinsen, O.M., 2013. Second-order diffraction and radiation of a floating body with small forward speed. *Journal of Offshore Mechanics and Arctic Engineering*, 135(1), pp.011301-011310.
- Shao, Y.L. and Helmers, J.B., 2014. Numerical analysis of second-order wave loads on large-volume marine structures in a current. *33rd International Conference on Ocean, Offshore and Arctic Engineering*, San Francisco, CA, 8-13 July 2014, pp.V01BT01A049.
- Skjoldal, S.O. and Faltinsen, O.M., 1980. A linear theory of springing. *Journal of Ship Research*, 24(2), pp.74-84.
- Slocum, S. and Troesch, A.W., 1983. *Nonlinear Ship Springing Experiments. Report No.266*. Ann Arbor: The University of Michigan, Department of Naval Architecture and Marine Engineering.
- Storhaug, G., 2007. *Experimental investigation of wave induced vibrations and their effect on the fatigue loading of ships*. Ph.D Thesis, Dept. Marine Technology, NTNU.
- Söding, H., 2009. Computation of springing transfer functions. *Proceedings of the Institution of Mechanical Engineers, Part M: Journal of Engineering for the Maritime Environment*, 223(3), pp.291-304.

- Tian, C. and Wu, Y.S., 2006. The non-linear hydroelastic responses of a ship travelling in waves. In: Y. S. Wu and W.C. Cui, ed. *Hydroelasticity in marine technology*. Beijing, China: National Defense Industry Press.
- Tuitman, J.T. and Malenica, S., 2009. Fully coupled seakeeping, slamming, and whipping calculations. *Proceedings of the Institution of Mechanical Engineers. Part M: Journal of Engineering for the Maritime Environment*. 223(3), pp.439-456.
- Vidic-Perunovics, J. and Jensen, J.J., 2005. Non-linear springing excitation due to a bidirectional wave field. *Marine Structures*, 18, pp.332-358.
- von Graefe, A., Moctar, O., Oberhagemann, J. and Shigunov, V., 2014. Linear and nonlinear sectional loads with potential and field methods. *Journal of Offshore Mechanics and Arctic Engineering*, 136(3), pp.031602-031611.
- Winterstein, S.R., Ude, T.C. and Marthinsen, T., 1994. Volterra models of ocean structures: Extreme and fatigue reliability. *Journal of Engineering Mechanics*, 120(6), pp.1369-1385.
- Wu, Y.S., Maeda, H. and Kinoshita, T., 1997. The second order hydrodynamic actions on a flexible body. *Journal of the Indian Institute of Science*, 49(4), pp.8-19.
- Zhao, R., Faltinsen, O. and Aarnes, J., 1997. Water entry of arbitrary two-dimensional sections with and without flow separation. *Proceedings of 21st Symposium on Naval Hydrodynamics*, Trondheim, Norway, 24-28 June 1996, pp. 408-423.

APPENDIX A

The transformation matrix $\mathbf{R}_{b \rightarrow i}$ in Eq. (4) is defined as

$$\mathbf{R}_{b \rightarrow i} = \begin{bmatrix} c_6 c_5 & c_6 s_5 s_4 - s_6 c_4 & c_6 s_5 c_4 + s_6 s_4 \\ s_6 c_5 & s_6 s_5 s_4 + c_6 c_4 & s_6 s_5 c_4 - c_6 s_4 \\ -s_5 & c_5 s_4 & c_5 c_4 \end{bmatrix}. \quad (\text{A.1})$$

Here $s_i = \sin(\alpha_i)$ and $c_i = \cos(\alpha_i)$ with $i=4, 5, 6$.

APPENDIX B

The forcing terms in the free surface conditions are defined as

$$f_1^{(1)} = \eta^{(1)} \phi_{zz}^{(0)} - (\phi_x^{(0)} \eta_x^{(1)} + \phi_y^{(0)} \eta_y^{(1)}) + U \eta_x^{(1)} - U_3^{r(1)}, \quad (\text{B.2})$$

$$f_1^{(2)} = \eta^{(2)} \phi_{zz}^{(0)} + \eta^{(1)} \phi_{zz}^{(1)} - (\phi_x^{(0)} \eta_x^{(2)} + \phi_y^{(0)} \eta_y^{(2)}) - (\phi_x^{(1)} \eta_x^{(1)} + \phi_y^{(1)} \eta_y^{(1)}) + U \eta_x^{(2)} + (U_1^{r(1)} \eta_x^{(1)} + U_2^{r(1)} \eta_y^{(1)}) - U_3^{r(2)} + (\chi_1^{(1)} \tilde{\eta}_x^{(1)} + \chi_2^{(1)} \tilde{\eta}_y^{(1)}) \quad (\text{B.3})$$

$$f_2^{(2)} = -\eta^{(1)} \phi_{zz}^{(1)} - \frac{1}{2} \nabla \phi^{(1)} \cdot \nabla \phi^{(1)} - \nabla \phi^{(0)} \cdot \nabla \phi^{(2)} - \eta^{(1)} (\nabla \phi_z^{(1)} \cdot \nabla \phi^{(0)} + \phi_{zz}^{(0)} \phi_z^{(1)}) + U \phi_x^{(2)} + U \eta^{(1)} \phi_{zz}^{(1)} + (\bar{\chi}^{(2)} + \bar{U}^{r(2)}) \cdot \nabla \phi^{(0)} + (\bar{\chi}^{(1)} + \bar{U}^{r(1)}) \cdot \nabla \phi^{(1)} + (\chi_3^{(1)} + U_3^{r(1)}) \eta^{(1)} \phi_{zz}^{(0)} \quad (\text{B.4})$$

Here $\bar{\chi}^{(1)}$ is the first-order velocity of a point on the free surface due to rigid-body motion, which is defined as

$$\bar{\chi}^{(1)} = (\chi_1^{(1)}, \chi_2^{(1)}, \chi_3^{(1)}) = (\dot{\xi}_1^{(1)} - y \dot{\alpha}_6^{(1)}) \vec{i} + (\dot{\xi}_2^{(1)} + x \dot{\alpha}_6^{(1)}) \vec{j} + (\dot{\xi}_3^{(1)} + y \dot{\alpha}_4^{(1)} - x \dot{\alpha}_5^{(1)}) \vec{k}. \quad (\text{B.5})$$

In this study, the forward speed is assumed to always parallel to the X-axis. In the inertial coordinate system OXYZ, the forward vector is $\vec{U}=U\vec{I}$ with \vec{I} the unit directional vector along the X-axis. However, when observed in the body-fixed coordinate system, it has components in x-, y- and z-directions due to the angular motions of the body. The forward speed vector in the body-fixed coordinate system \vec{U}' can be obtained approximated as

$$\vec{U}' = \vec{U}'^{(0)} + \vec{U}'^{(1)} + \vec{U}'^{(2)} + O(\varepsilon^3), \tag{B.6}$$

where

$$\vec{U}'^{(0)} = U \begin{bmatrix} 1 \\ 0 \\ 0 \end{bmatrix}, \quad \vec{U}'^{(1)} = \begin{bmatrix} U_1^{(1)} \\ U_2^{(1)} \\ U_3^{(1)} \end{bmatrix} = U \begin{bmatrix} \mathbf{0} \\ -\alpha_6^{(1)} \\ \alpha_5^{(1)} \end{bmatrix}, \quad \vec{U}'^{(2)} = \begin{bmatrix} U_1^{(2)} \\ U_2^{(2)} \\ U_3^{(2)} \end{bmatrix} = U \begin{bmatrix} -\frac{1}{2}[(\alpha_5^{(1)})^2 + (\alpha_6^{(1)})^2] \\ -\alpha_6^{(2)} + \alpha_4^{(1)}\alpha_5^{(1)} \\ \alpha_5^{(2)} + \alpha_4^{(1)}\alpha_6^{(1)} \end{bmatrix}. \tag{B.7}$$